Terahertz time-domain spectroscopy characterization of the far-infrared absorption and index of refraction of high-resistivity, float-zone silicon

Jianming Dai, Jiangquan Zhang, Weili Zhang, and D. Grischkowsky

School of Electrical and Computer Engineering, Oklahoma State University, Stillwater, Oklahoma 74078

Manuscript received August 25, 2003; revised manuscript received February 6, 2004; accepted February 6, 2004

The far-infrared absorption and index of refraction of high-resistivity, float-zone, crystalline silicon has been measured by terahertz time-domain spectroscopy. The measured new upper limit for the absorption of this most transparent dielectric material in the far infrared shows unprecedented transparency over the range from 0.5 to 2.5 THz and a well-resolved absorption feature at 3.6 THz. The index of refraction shows remarkably little dispersion, changing by only 0.0001 over the range from 0.5 to 4.5 THz. © 2004 Optical Society of America

OCIS codes: 320.0320, 300.0300, 300.6270, 250.0250.

At the present time, the most transparent dielectric material in the terahertz (THz) frequency region (far-infrared) is high-resistivity, float-zone (FZ) single-crystal silicon. In addition, the index of refraction is essentially constant, showing little dispersion from 35 GHz to 4 THz. Consequently, this material has found extensive use as windows, quasi-optic lenses, and dielectric cavities. Other applications, depending on the limiting absorption of this material, would include THz single-crystal, single-mode, dielectric fiber waveguides and planar slab or ribbon waveguides. Because the absorption of pure intrinsic silicon is so low in the frequency range from 0.1 to 4 THz, all previous measurements have been upper limits to the intrinsic absorption.[1–14] The purpose of this terahertz time-domain spectroscopy (THz-TDS) investigation is to provide measurements that approach the intrinsic absorption and dispersion limit of FZ-Si. Here, we report the highest measured transparency and the most accurate measurement of the index of refraction for float-zone silicon to date. These results will enable realistic assessment of new applications using this material.

The significant literature of far-infrared measurements on silicon illustrates the importance of using well understood and well-characterized samples, coupled with careful experimental procedures.[1–14] Below 4 THz, there are noteworthy discrepancies among the published data, with variations in the measured absorption coefficients of up to 5 times. The main reason for these inconsistent results is that, below 1.5 THz, the measurements are extremely sensitive to the presence of carriers. For relatively low dopings with resistivities greater than 10 Ω cm, the absorption below 1.5 THz is proportional to carrier density and thereby inversely proportional to resistivity. Recent measurements have shown that for 8-Ω cm, *n*-type silicon, the peak low-frequency power absorption coefficient is $\alpha = 13\ \mathrm{cm}^{-1}$,[11] and for 320-Ω cm, *n*-type silicon, the peak value is $\alpha = 0.34\ \mathrm{cm}^{-1}$.[14] Extrapolation of these values yields the following peak absorptions: 1 kΩ cm, $\alpha = 0.1\ \mathrm{cm}^{-1}$; and for 10 kΩ cm, $\alpha = 0.01\ \mathrm{cm}^{-1}$. Consequently, unless high-purity, high-resistivity material is used, what is measured is not the properties of intrinsic silicon, but of the carriers due to the residual impurities. This problem is most prevalent in the earlier work on silicon with a resistivity of 10 Ω cm[1] to 100 Ω cm.[2] Later work measured samples with resistivities of 8 kΩ cm,[6] 1.5 kΩ cm,[7] and 11 kΩ cm.[12]

The first high-resistivity, float-zone silicon samples measured by THz-TDS had resistivities higher than 10 kΩ cm; for this material, a record transparency was measured together with a remarkably flat dispersion curve.[10] Throughout the range from low frequencies to 2 THz, the measured absorption coefficient for silicon was less than $0.05\ \mathrm{cm}^{-1}$, and the index of refraction $n = 3.418$ changed by less than ±0.001. The only results consistent with this early THz-TDS measurement[10] are those in Ref. 8. As an illustration of the previous wide range of values, even though the measurements of Ref. 6 were made on a high-resistivity, 8-kΩ cm silicon sample, they gave the significantly higher and strongly frequency-dependent absorption coefficient between 0.2 and 0.4 THz of approximately $0.13\ \mathrm{cm}^{-1}$; this discrepancy was ascribed to the higher quality of silicon used for the THz-TDS measurement.[10] Another work made a single-point measurement at 0.245 THz on a 1.5-kΩ cm silicon sample and measured an index of refraction of $n = 3.418$ and an absorption coefficient of $0.13\ \mathrm{cm}^{-1}$.[7] The work of Ref. 12 used a high-resistivity (11-kΩ) silicon sample that had been compensated by boron doping. The measured power-absorption coefficient was approximately 0.005 cm^{-1} at 0.12 THz, increasing to 0.01 cm^{-1} at 0.18 THz

0740-3224/2004/071379-08$15.00

and equal to 0.05 cm^{-1} at 0.3 THz, then increasing rapidly to 0.11 cm^{-1} at 0.45 THz, the measurement limit. This rapid increase in absorption is tentatively ascribed to a decrease in crystal quality due to the boron compensation, compared with the float-zone silicon.

In the work reported here, we have set a new measured upper limit for the intrinsic absorption of high-resistivity, float-zone silicon showing unprecedented transparency over the range from 0.5 to 2.5 THz and observed a well-resolved absorption feature at 3.6 THz. The index of refraction showed remarkably little dispersion, changing by only 0.0001 over the range from 0.5 to 4.5 THz. These THz-TDS measurements were made with the experimental setup shown in Fig. 1. The setup consists of an optoelectronic transmitter and receiver together with beam shaping and steering optics and is situated in an enclosure maintained at a relative humidity of less than 1% to mitigate the effects of water vapor. A detailed description of the entire THz-TDS system has been previously published.[10] For the usual case of THz-TDS measurements, two electromagnetic pulse shapes are measured: the reference pulse without the sample in the system, and the sample pulse, which has changed shape due to its passage through the sample under study. Consequently, through a complex numerical Fourier analysis of the reference and sample pulses, the frequency-dependent absorption and dispersion of the sample can be obtained. This relatively simple approach assumes that the change in the power transfer function[15] from the transmitter to the receiver due to the insertion of the sample is negligible compared with the absorption and dispersive effects due to propagation through the sample. However, because of the very low absorption of FZ-Si, relatively small changes in the power transfer function are an important experimental consideration.

The standard THz beam system has symmetric confocal optics with respect to the center line of the system between the transmitter and receiver. The transmitting antenna is at the focus of the silicon lens, which collimates the complicated frequency-independent far-field pattern of the Hertzian dipole antenna to an approximately 1/*e* amplitude beam-waist diameter of 4 mm. This is beam waist W1 shown in Fig. 1. This beam waist is in turn in the focal plane of the transmitter paraboloidal mirror, which focuses the THz beam to the second beam waist W2 with beam diameters proportional to wavelength. The THz optical system is identical (but reversed) from this point on to the receiver. For a Gaussian beam, this situation would give a unity, frequency-independent, power-coupling efficiency between the transmitter and receiver with no sample in place (see Eq. 2.16, Ref. 15). Unfortunately, recent work has shown that the previous oversimplified assumption that the entire THz beam can be approximated by a Gaussian beam is incorrect and has shown that the confocal arrangement does not have unity power transfer for this complicated beam.[16] In our case, to minimize the sample effect on the power transfer function, the sample is centered on the THz beam waist W2. However, for large-index dielectric samples with lengths of many centimeters, the change in the power transfer function can be significant with respect to the measurement of materials with very low absorptions.

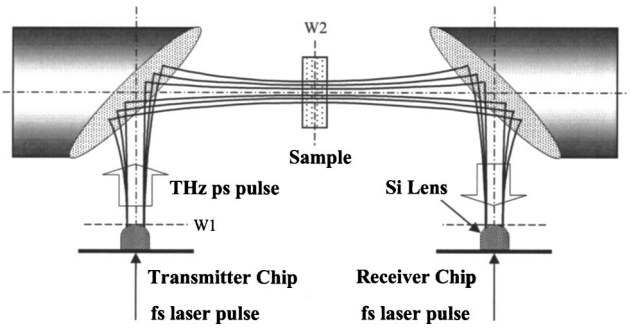

Fig. 1. The optoelectronic THz-TDS confocal quasi-optic system.

In order to overcome these experimental problems due to the changing power transfer function, the previous THz-TDS measurements of a 15-cm-long, 7.6-cm-diameter cylinder of 320-Ω cm, neutron-doped FZ silicon used the following approach.[14] First, the amplitudes of freely propagating subpicosecond THz electromagnetic signal pulses transmitted through the 320-Ω cm silicon sample were measured. These transmitted pulses were then compared with the measured THz reference pulses with the sample replaced by an identical cylinder of high resistivity, greater than 5-kΩ cm, FZ silicon with a residual carrier density of less than $N = 5 \times 10^{11}/cm^3$, less than 1/10 that of the sample carrier density. Using this procedure, the power transfer function of the THz-TDS system was unchanged for the reference and sample pulses, because the measurements were directly compared with an identical high-resistivity, FZ-Si cylinder. The maximum frequency-dependent difference between the index of refraction of the two cylinders was less than 0.003. This procedure allowed the measurement of the extremely small absorption on the high-frequency wing of the sample response.

Unfortunately, the above procedure is not possible for measurements of high-resistivity FZ silicon itself, because there is no reference dielectric with lower loss. Our initial investigation involved measuring a series of THz signal pulses transmitted through FZ-Si samples with lengths ranging from 10 mm to 150 mm, together with THz reference pulses taken with the samples removed. For these samples, a correction would need to be calculated to accommodate the change in the power-transfer function of the THz-TDS system due to the insertion of a lossless dielectric with the same shape and dielectric constant of the sample. However, for the complicated shape of the actual THz beam[16] the power transfer function corrections are comparable to the sample absorption, and the experimental uncertainties involved in the power transfer calculations led to inconsistencies between the various samples. Consequently, it was not possible to make reliable corrections for changes in the transfer function.

In order to assess the relative importance of the power transfer function, our measurements were performed in three different ways on combinations of different samples of FZ-Si. Initially we will discuss the samples and then the three different measurement methods.

For this experiment we used combinations of four FZ-Si plates, 5.1-cm diameter, 9.805 ± 0.005 mm thick with an

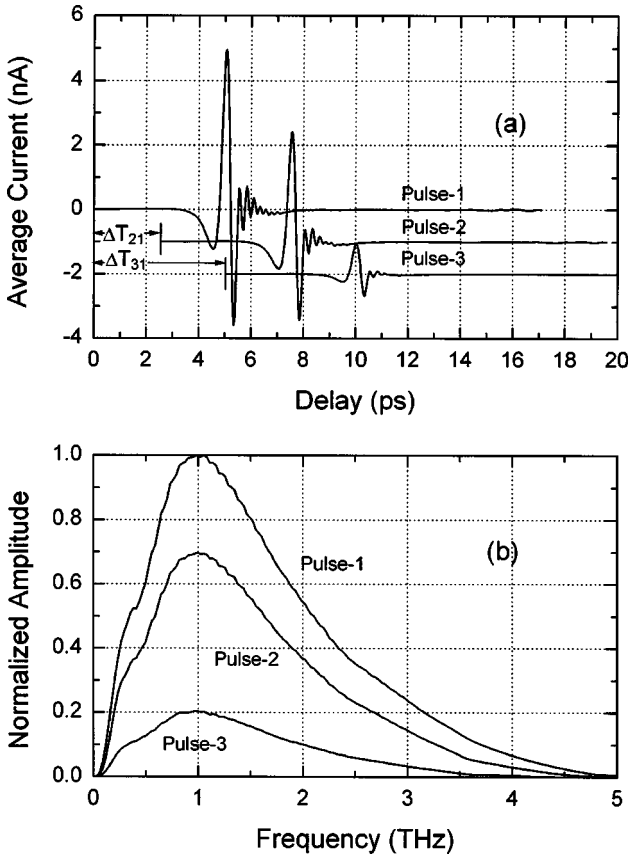

Fig. 2. (a) Measured transmitted pulses 1–3. (b) Corresponding amplitude spectra for pulses 1–3.

optical polish on both surfaces. These plates were obtained from Topsil Semiconductor Materials more than 10 years ago and are specified to have a resistivity of more than 10 kΩ cm. In order to achieve lengths of 19.61 mm and 39.22 mm, two and four plates were optically contacted together. Although we present measurements for the four-plate sample only, consistent results were obtained with the single and double plate samples. The contact plane between plates showed amplitude reflections of less than 0.3 percent, corresponding to a power reflection of only 0.9×10^{-5}. The plates could be later separated if desired. One remaining experimental problem was that two of the plates were slightly wedged with an angle of 0.15 mrad (0.00015 rad). However, the effect of the two wedged plates could be canceled, by optically contacting the plates together with the wedges opposed in the two-plate or four-plate sample configuration. In order to make a measurement, the THz-TDS system was initially aligned to achieve maximum signal and bandwidth. The sample was then put in place and oriented perpendicular to the input THz beam by monitoring the peak of the transmitted reference pulse and adjusting the sample tilt to move this peak to the earliest time. Then the measurement was performed. Experimentally, it was found that to achieve self-consistent results with this technique, the sample faces needed to be optically polished. On other samples, the standard lapped finish caused additional loss for the reflected THz sample pulse. This surface sensitivity is presumed to be due to the two surface reflections of one of the to-be-discussed configurations for the sample pulse, in contrast to the relative insensitivity of the directly transmitted reference pulse. Another experimental requirement was surface cleanliness of the plates, which were carefully cleaned in acetone before assembly.

In order to perform our THz-TDS characterizations, three different pulses were measured, the usual reference pulse, here designated as the transmitted pulse 1 through the system with no sample in place, the usual sample pulse, designated as the transmitted pulse 2 with the sample in place, and the double internally reflected pulse 3, which has traversed the sample three times and is transmitted in the forward direction. These three pulses, which are the averages of seven individual pulses and their corresponding amplitude spectra, are shown in Fig. 2. The three pulses illustrate the excellent signal-to-noise ratio and the fast response of the THz-TDS system. If there were no absorption by the sample and the index of refraction was constant at $n = 3.417$, all the pulses would have identical pulse shapes and spectra, but the amplitude of pulse 2 would be $t_{12}t_{21} = 0.701$ that of the pulse 1, and the amplitude of pulse 3 would be $t_{12}r_{21}r_{21}t_{21} = 0.210$ that of the pulse 1. The same three pulses are again shown in Fig. 3, where pulse 1 and its spectrum were unchanged; pulse 2 and its spectrum were divided by 0.701, and pulse 3 and its spectrum were divided by 0.210 to enable better comparison between the pulses. Here, we can observe the small comparative frequency-dependent amplitude reduction of the sample

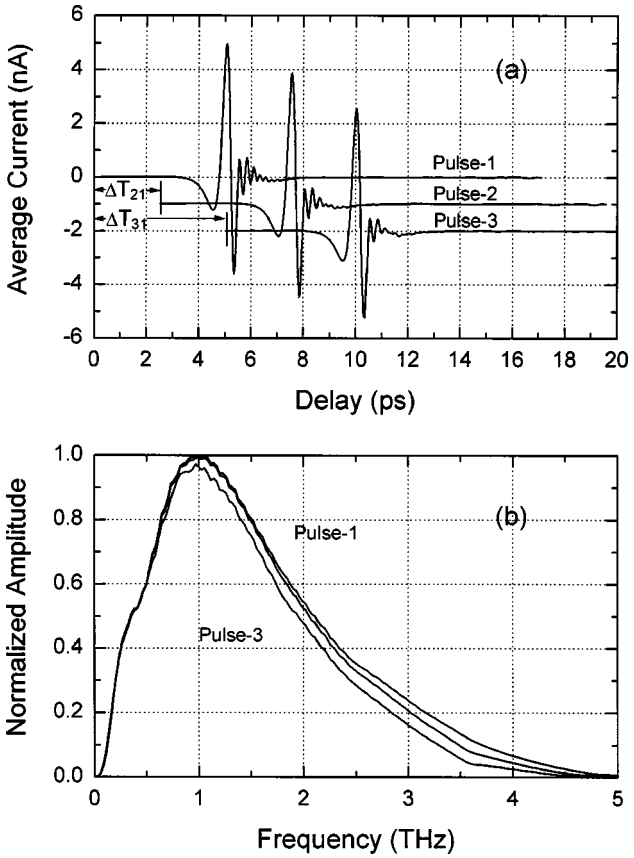

Fig. 3. (a) Measured transmitted pulses: Pulse 1, (Pulse 2)/$(t_{12}t_{21})$, (Pulse 3)/$(t_{12}r_{21}r_{21}t_{21})$. (b) Amplitude spectra for Pulse 1, (Pulse 2)/$(t_{12}t_{21})$, (Pulse 3)/$(t_{12}r_{21}r_{21}t_{21})$.

pulses due to the absorption of the FZ-Si sample and to the changes in the power transfer function.

These three pulses are described in the frequency domain by their complex amplitude spectra $A_1(\omega)$, $A_2(\omega)$, and $A_3(\omega)$, in Eqs. (1a), (1b), and (1c), respectively:

$$A_1(\omega) = |A_1(\omega)|\exp[i\phi_1(\omega)] = A_o(\omega)U_1(\omega)\exp[ik_o(\omega)L], \quad (1a)$$

$$A_2(\omega) = |A_2(\omega)|\exp[i\phi_2(\omega)] = A_o(\omega)U_2(\omega)t_{12}t_{21}\exp[-\alpha(\omega)L/2]\exp[ik(\omega)L], \quad (1b)$$

$$A_3(\omega) = |A_3(\omega)|\exp[i\phi_3(\omega)] = A_o(\omega)U_3(\omega)t_{12}r_{21}r_{21}t_{21}\exp[-3\alpha(\omega)L/2] \times \exp[i3k(\omega)L], \quad (1c)$$

where $A_o(\omega)$ is the complex spectral amplitude incident on the sample of length L. The Fresnel transmission coefficients of the sample interfaces are designated as t_{12} and t_{21} with the subscript 1 referring to air and 2 referring to FZ-Si; r_{21} is the Fresnel reflection coefficient from the silicon/air interface; $\alpha(\omega)$ is the desired power absorption coefficient, and $k(\omega) = 2\pi n(\omega)/\lambda_o$ with $n(\omega)$ the desired index of refraction; $k_o = 2\pi n_{Air}(\mathrm{THz})/\lambda_o$, where λ_o is the wavelength in free space and $n_{Air}(\mathrm{THz}) = 1.00027$ is the index of dry air at THz frequencies. $U_1(\omega)$, $U_2(\omega)$, and $U_3(\omega)$ are the complex-amplitude transfer functions of the THz system for pulses 1–3, respectively. The corresponding power transfer functions $P_1(\omega)$, $P_2(\omega)$, and $P_3(\omega)$ are given by $U_1(\omega)U_1(\omega)^*$, $U_2(\omega)U_2(\omega)^*$, and $U_3(\omega)U_3(\omega)^*$, respectively, where the superscript* indicates complex conjugate.

From Eqs. (1), we form the ratios of Eqs. (2), which will be used to obtain our THz-TDS characterizations of FZ-Si:

$$A_2(\omega)/A_1(\omega) = [U_2(\omega)/U_1(\omega)]t_{12}t_{21}\exp[-\alpha(\omega)L/2] \times \exp[i(k(\omega) - k_o)L], \quad (2a)$$

$$A_3(\omega)/A_1(\omega) = [U_3(\omega)/U_1(\omega)]t_{12}r_{21}r_{21}t_{21} \times \exp[-3\alpha(\omega)L/2] \times \exp[i(3k(\omega) - k_o)L], \quad (2b)$$

$$A_3(\omega)/A_2(\omega) = [U_3(\omega)/U_2(\omega)]r_{21}r_{21}\exp[-\alpha(\omega)L] \times \exp[i2k(\omega)L]. \quad (2c)$$

Knowing that the absorption of FZ-Si is very low, the Fresnel coefficients t_{12}, t_{21}, and r_{21} have a negligible complex component. We also expect that U_1, U_2, and U_3 have small complex terms. The measured phase angles given by the ratios of the complex spectra as described by Eqs. (2) enable us to determine the index of refraction n_{Si} of FZ-Si. However, before we can do this, we must discuss some experimental details about how these phase data are obtained.

Although time-shifted pulses 1–3 appear to overlap in time, through our computer-controlled stepping-motor delay line, we know that the starting position of the scan for pulse 2 is delayed from that of pulse 1 by $\Delta T_{21} = 316.317$ ps and that the scan for pulse 3 is delayed from that of pulse 1 by $\Delta T_{31} = 1210.775$ ps. These time shifts are given by the relationship $\Delta T_{21} = 2(L_2 - L_1)n_{Air}(\mathrm{vis.})/c$, where L_2 is the delay-line start position for pulse 2, L_1 that for pulse 1, and $n_{Air}(\mathrm{vis.}) = 1.00027$ is the index of refraction of air at 1 atm, room temperature, 40% humidity, and 800 nm; the given value for $n_{Air}(\mathrm{vis.})$ does not change with ± 5 °C changes in temperature or $\pm 10\%$ changes in humidity. $c = 2.99793 \times 10^{10}$ cm/s is the speed of light in vacuum. The stepper-motor delay-line system (Newport MTM250PP.1) is usually set to make 5-μm steps. The system has an accuracy and resetability of ± 0.2 μm. This situation is described by the following equations:

$$[\phi_2(\omega) - \phi_1(\omega)] \equiv (2\pi/\lambda_o)[n_{21}(\omega) - n_{Air}(\mathrm{THz})]L - \omega\Delta T_{21}, \quad (3a)$$

$$[\phi_3(\omega) - \phi_1(\omega)] \equiv (2\pi/\lambda_o)[3n_{31}(\omega) - n_{Air}(\mathrm{THz})]L - \omega\Delta T_{31}, \quad (3b)$$

$$[\phi_3(\omega) - \phi_2(\omega)] \equiv (2\pi/\lambda_o)2n_{32}(\omega)L - \omega\Delta T_{32}, \quad (3c)$$

which define the indices $n_{21}(\omega)$, $n_{31}(\omega)$, and $n_{32}(\omega)$, where the small phase angles of the corresponding ratios of the transfer functions are included in these indices. These equations are much more precise to determine the frequency dependence of the index, because the very large phase terms due to the different transit times through the samples have been accurately subtracted off experimentally by the precision delay line.

In the initial analysis, the weakly frequency-dependent indices $n_{21}(\omega)$, $n_{31}(\omega)$, and $n_{32}(\omega)$ determined by Eqs. (3a), (3b), and (3c), respectively, slightly disagreed, although they were all within the range from 3.4180 to 3.4184 for frequencies between 0.5 THz and 4.5 THz. These results were achieved by assigning a total sample length of $L = 39.222$ mm. However, we cannot measure our individual plate thicknesses to better than ± 5 μm; thus our length is uncertain on the scale of ± 10 μm. When the sample thickness was changed by micron-step sizes in the analysis, the three measurements came into precise agreement at the length of $L = 39.231$ mm. This intersection occurred owing to the different dependence on length L, as shown in Eqs. (3), for which precise agreement between the three values of the index will occur for only the correct value of L. This situation is similar to that reported in an earlier experiment.[17] Extremely accurate data are required to enable the determination of both the correct length of the sample and the corresponding measurement of the index. This remarkable result shown in Fig. 4 illustrates the accuracy and reproducibility of the phase measurement. It also shows that from 0.5 to 4 THz, the phase angles associated with the transfer functions are less than 10 mrad, as evidenced by the slight differences between the index curves. Here, one can see the extremely weak frequency dependence of the index over the frequency range from 0.5 to 4.5 THz, where the index monotonically increases from 3.41745 at 0.5 THz to 3.41753 at 3 THz, followed by a small but distinct resonance feature at 3.66 THz. This weak resonance has been previously observed by an absorption measure-

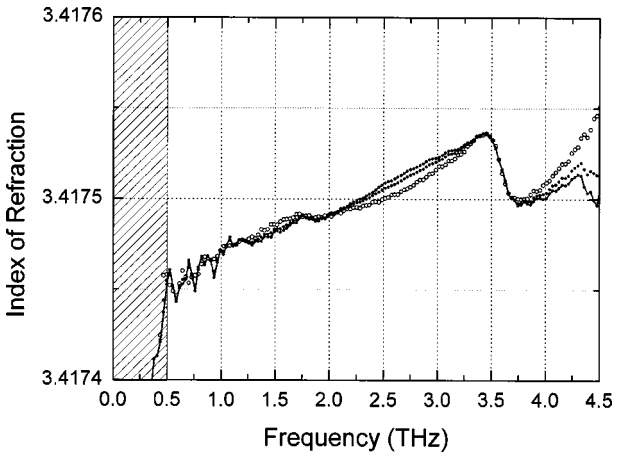

Fig. 4. Measured indices of refraction, n_{21} (open circles), n_{31} (dots), n_{32} (connected dots). These measurements are considered accurate between 0.5 THz and 4.5 THz.

ment.[5] As will be discussed in more detail, we believe that $U_3(\omega)/U_2(\omega)$ is very close to unity, and therefore the curve $n_{32}(\omega)$ is our most accurate measure of $n(\omega)$, the index of refraction of high-resistivity, float-zone silicon.

Although we believe the very low dispersion (frequency dependence) of the measured index to be correct, because of possible unresolved frequency-independent systematic experimental effects, we consider the indicated index values to be accurate to ± 0.0002. Thus the entire curve shown in Fig. 4 could move up or down by ± 0.0002. Possible systematic concerns are the accuracy of the index of refraction of air at 800 nm and THz frequencies and the associated effects of temperature, air pressure, and humidity. We consider the values for air used in our analysis to be accurate to $\pm 10\%$. Accuracy of the precise length of travel of the delay line and associated effects of thermal expansion are of concern. In addition, the thermal dependence of the index of silicon and a possible small phase shift between the silicon plates are a source of possible error.

From Eqs. (2), it is easy to solve explicitly for the absorption coefficient:

$$\alpha(\omega) = (2/L)\mathrm{Ln}|U_2(\omega)/U_1(\omega)| - (2/L)\mathrm{Ln}[|A_2(\omega)/A_1(\omega)|/(t_{12}t_{21})], \quad (4a)$$

$$\alpha(\omega) = [2/(3L)]\mathrm{Ln}|U_3(\omega)/U_1(\omega)| - [2/(3L)]\mathrm{Ln}[|A_3(\omega)/A_1(\omega)|/(t_{12}r_{21}r_{21}t_{21})], \quad (4b)$$

$$\alpha(\omega) = (1/L)\mathrm{Ln}|U_3(\omega)/U_2(\omega)| - (1/L)\mathrm{Ln}[|A_3(\omega)/A_2(\omega)|/(r_{21}r_{21})]. \quad (4c)$$

The heart of the measurement problem for absorption is obtaining the ratios of the unknown transfer functions in Eqs. (4). If the effect of the transfer functions were small compared with the measured absorption, they could be neglected. If they were the same for the different sample configurations, they would cancel out of the measurement. The ratio described by Eq. (2c) for the reflection method uses the directly transmitted incident pulse through the sample as the reference pulse and the first reflected pulse in the output pulse train as the sample pulse. Because this method does not require any movement of the sample and the actual physical length L of the sample is smaller than the effective measurement length $3L$ owing to the use of multiple reflections, it was expected to have a significantly smaller power transfer-function effect. As will be discussed below, we have performed a self-consistent analysis to set an upper limit to $\alpha(\omega)$, based on this intuitive assumption. First, we define the new absorption coefficients $\alpha_{21}(\omega)$, $\alpha_{31}(\omega)$, and $\alpha_{32}(\omega)$ that formally include the transfer functions as shown below:

$$|A_2(\omega)/A_1(\omega)| \equiv t_{12}t_{21}\exp[-\alpha_{21}(\omega)L/2], \quad (5a)$$

$$|A_3(\omega)/A_1(\omega)| \equiv t_{12}r_{21}r_{21}t_{21}\exp[-3\alpha_{31}(\omega)L/2], \quad (5b)$$

$$|A_3(\omega)/A_2(\omega)| \equiv r_{21}r_{21}\exp[-\alpha_{32}(\omega)L]. \quad (5c)$$

These three absorption coefficients are given explicitly below and are related to the desired absorption coefficient $\alpha(\omega)$:

$$\alpha_{21}(\omega) = -(2/L)\mathrm{Ln}[|A_2(\omega)/A_1(\omega)|/(t_{12}t_{21})] = \alpha(\omega) - (2/L)\mathrm{Ln}|U_2(\omega)/U_1(\omega)|, \quad (6a)$$

$$\alpha_{31}(\omega) = -[2/(3L)]\mathrm{Ln}[|A_3(\omega)/A_1(\omega)|/(t_{12}r_{21}r_{21}t_{21})] = \alpha(\omega) - [2/(3L)]\mathrm{Ln}|U_3(\omega)/U_1(\omega)|, \quad (6b)$$

$$\alpha_{32}(\omega) = -(1/L)\mathrm{Ln}[|A_3(\omega)/A_2(\omega)|/(r_{21}r_{21})] = \alpha(\omega) - (1/L)\mathrm{Ln}|U_3(\omega)/U_2(\omega)|. \quad (6c)$$

Using the three pulses and their corresponding amplitude spectra shown in Fig. 3, we calculate the three absorption coefficients defined in Eqs. (5) and (6), which include the ratio of the amplitude transfer functions. The resulting frequency-dependent power absorption coefficients α_{21}, α_{31}, and α_{32} determined from our experimental data are displayed in Fig. 5. The deviation of these curves from one another is due to the different transfer-function relationships included in the three curves. The results shown in Fig. 5 clearly demonstrate the effects of changes of the system transfer function caused by the insertion of high dielectric-constant samples placed in the

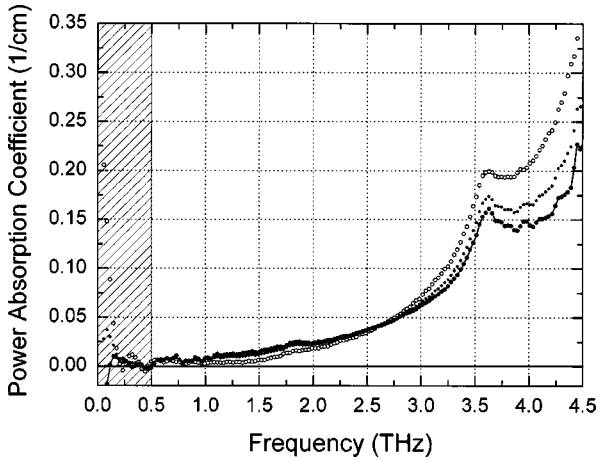

Fig. 5. Measured power absorption coefficients $\alpha_{21}(\omega)$ open circles, $\alpha_{31}(\omega)$ dots, and $\alpha_{32}(\omega)$ connected dots. These measurements are considered accurate between 0.5 THz and 4.5 THz.

standard THz-TDS system. However, from the relatively small magnitude of the effects, it can be seen that, for the usual type measurements of much higher absorption coefficients, these changes can be ignored, but not for the work presented here.

The measured intersection at 2.60 THz is relatively sharp and well defined; here we consider that all the transfer functions have the same value and that the absorption coefficients are equal to the intrinsic absorption coefficient $\alpha(\omega)$. This assumption is physically reasonable and is a mathematical solution of Eqs. (6), but is not the only solution. This assumption will be given more credibility by the additional measurements discussed below and made with different samples and with different THz beams.

From equations (6), it is clear that if the quantities $\mathrm{Ln}|U_2(\omega)/U_1(\omega)|$, $\mathrm{Ln}|U_3(\omega)/U_1(\omega)|$, and $\mathrm{Ln}|U_3(\omega)/U_2(\omega)|$ are negative, indicating that the transfer function for the reference pulse is closer to unity than that of the signal pulse, the measured absorption coefficients $\alpha_{21}(\omega)$, $\alpha_{31}(\omega)$, and $\alpha_{32}(\omega)$ will be upper limits to the absorption $\alpha(\omega)$; the converse applies if the quantities are positive. In addition, the absorption $\alpha(\omega)$ is obtained at the crossing points of 0.5 and 2.6 THz, shown in Fig. 5. Other measurements taken with a single plate show a crossing point at 3 THz, which gives a measure of $\alpha(\omega)$ in agreement with $\alpha_{32}(\omega)$ in Fig. 5. As discussed above, we consider that $|U_3(\omega)/U_2(\omega)|$ is the ratio closest to unity. We also consider that above the 2.6 THz crossing point, the ratios $|U_2(\omega)/U_1(\omega)|$ and $|U_3(\omega)/U_1(\omega)|$ are less than unity, but that below this point, until the crossing point at 0.5 THz, they are greater than unity, indicating that within this frequency range the transfer function is closer to unity with a sample in place than without.

This opinion is supported by an additional series of measurements with a different THz beam profile achieved by placing 4-mm-diameter apertures in front of the silicon lenses of the transmitter and receiver. The resulting measurements are similar to Fig. 5, indicating that the goal to achieve more efficient transfer functions by transmitting only the main lobe of the emitted beam was not achieved. However, these measurements do have an intersection point at 1.5 THz, thereby giving another measurement of $\alpha(\omega)$, which agrees with $\alpha_{32}(\omega)$ shown in Fig. 5. Consequently, we consider $\alpha_{32}(\omega)$ to be an accurate upper limit to the intrinsic power absorption coefficient $\alpha(\omega)$ of high-resistivity, float-zone silicon. In Fig. 6(a), we present $\alpha_{32}(\omega)$ as this upper limit. A similar logic holds for the index of refraction for which the transfer-function effects are much smaller; consequently, we present $n_{32}(\omega)$ in Fig. 6(b) as the most accurate measurement to date of $n(\omega)$.

With respect to the experimental error in the measurements of the absorption coefficient $\alpha(\omega)$ and the index of refraction $n(\omega)$ as shown in Figs. 6(a) and 6(b), the following considerations apply. For our system, each presented data point logically corresponds to an independent measurement. Consequently, the measurement error is indicated by the data scatter, which for most of the length of the presented curves for $\alpha(\omega)$ and $n(\omega)$ is seen to be less than the diameter of the plotted points.

Our main source of experimental error is the relatively slow variations of the generated THz pulses with respect to their amplitude and phase. Our data-taking procedure to minimize this problem will now be described. Before initiating a series of measurements, the THz system was stabilized until the fluctuation of the peak spectral amplitude at 1 THz of any one of ten consecutive measurements of the reference THz pulse (pulse 1) was less than ± 0.5 percent. The measurement of a single pulse took 250 seconds. After this stabilization, the data-taking sequence was initiated. We first measured the reference pulse (pulse 1 with no sample in the system). The sample was then moved into position without letting any water vapor into the sealed experimental enclosure, and pulse 2 was measured. Finally, pulse 3 was measured. This sequence was repeated seven times, in order to obtain a complete data set for which all the corresponding pulses were averaged together. Figure 2 shows such an averaged data set for the three pulse types. Before accepting a data set, the amplitude spectra of the individual pulses were compared with the amplitude spectrum of the averaged pulse.

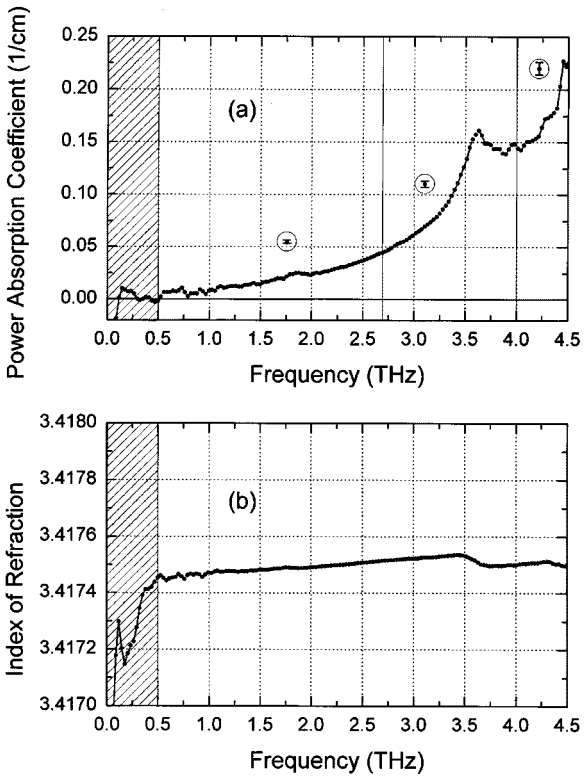

Fig. 6. (a) Upper limit $\alpha_{32}(\omega)$ to the power absorption coefficient $\alpha(\omega)$ of float-zone, high-resistivity silicon. The estimated experimental error in $\alpha_{32}(\omega)$ is ± 0.0015 cm^{-1} in the region from 0.5 to 2.7 THz, ± 0.003 cm^{-1} in the region from 2.7 to 4 THz, and ± 0.006 cm^{-1} in the region from 4 to 4.5 THz. These frequency regions are located between the vertical dashed lines together with the corresponding calibration points centered in the circles indicating the experimental error. (b) Measured index of refraction $n_{32}(\omega)$. The estimated experimental error of ± 0.00001 for the frequency dependence of the index of refraction $n_{32}(\omega)$ is smaller than the data-point diameters shown in Fig. 6(b); although because of possible unresolved frequency-independent, systematic experimental effects, the entire curve shown in Fig. 6(b) could move up or down by ± 0.0002. These measurements are considered accurate between 0.5 THz and 4.5 THz.

A comparison of the measured amplitude spectra of the individual members of the data set divided by the amplitude spectrum of the averaged pulse shows that the individual spectra deviate from the average spectrum by less than $\pm 0.5\%$ from 0.5 to 2.7 THz, by less than $\pm 1\%$ from 2.7 to 4 THz, and by less than $\pm 2\%$ from 4 to 4.5 THz. A similar comparison of the corresponding relative phase of the individual members of the data set to the phase of the averaged pulse shows that the individual phase variations are less than $\pm 0.015f$ radians, where f is the frequency in THz ($f = 1$ at 1 THz). Assuming random variations, the average of the seven-member data set reduces the above individual deviations by the factor $1/\sqrt{7}$. Consequently, the deviations for the average spectrum become less than $\pm 0.2\%$ from 0.5 to 2.7 THz, less than $\pm 0.4\%$ from 2.7 to 4 THz, and by less than $\pm 0.8\%$ from 4 to 4.5 THz. Similarly, the deviations of phase of the averaged pulse are considered to be less than $\pm 0.006f$ radians. Again considering random deviations, for the ratio of the pulse amplitude spectra used to calculate the absorption, the above values are increased by $\sqrt{2}$. Therefore the deviation of the ratio becomes less than $\pm 0.3\%$ from 0.5 to 2.7 THz, less than $\pm 0.6\%$ from 2.7 to 4 THz, and less than $\pm 1.2\%$ from 4 to 4.5 THz. Similarly, the deviations of phase ratio used to calculate the index of refraction are considered to be less than $\pm 0.01f$ radians.

Because we are in the limit of small absorption, the deviation in $\alpha(\omega)\, L/2$ is given by that of the ratio of the amplitude spectra. Consequently the estimated experimental error in $\alpha(\omega)$ is ± 0.0015 cm^{-1} in the region from 0.5 to 2.7 THz, ± 0.003 cm^{-1} in the region from 2.7 to 4 THz, and ± 0.006 cm^{-1} in the region from 4 to 4.5 THz. These frequency regions are located between the vertical dashed lines in Fig. 6(a) together with the corresponding calibration points centered in the circles indicating our estimated experimental error in these regions. The corresponding deviation δ_n in the index of refraction $n(\omega)$ is given by the relationship $\pm 0.01f = 2\pi\delta_n L/\lambda_0$. Evaluating this relationship yields $\delta_n = \pm 0.00001$ for the estimated experimental error of the index of refraction, which is smaller than the data-point diameters shown in Fig. 6(b). However, because of possible unresolved frequency-independent, systematic experimental effects discussed above, the entire curve shown in Fig. 6(b) could move up or down by ± 0.0002.

Compared with the previous work, these absorption results are dramatically lower and cover a broader frequency range. The first THz-TDS measurement[10] of FZ-Si set an upper limit to the power absorption coefficient $\alpha < 0.05$ cm^{-1} for frequencies below 2 THz, which is clearly consistent with Fig. 6(a). The fact that the measured absorption upper limit $\alpha_{32}(\omega)$ is less than 0.01 cm^{-1} in the frequency band from 0.2 to 1 THz and is less than 0.025 cm^{-1} in the frequency band from 0.2 to 2 THz is quite significant. This result lowers by the factor 2 the previous upper limit[10] for $\alpha(\omega)$ over this frequency range. There exists no other dielectric material with a comparable transparency. The relatively rapid rise in absorption as the frequency is increased from 1.5 THz appears to be due to two previously reported weak absorption bands at 3.66 and 4.68 THz[5] and not due exclusively to the main phonon band at 18 THz.

In conclusion, although our measurements were complicated by the fundamental problem of changes in the power transfer function of the THz-TDS spectrometer due to the insertion of the high-index silicon samples into our apparatus, we were able to measure unprecedented transparency and an essentially nondispersive index of refraction for high-resistivity, float-zone crystalline silicon (FZ-Si). We have set a new measured upper limit for the intrinsic absorption of this material over the range from 0.5 to 4.5 THz and observed a well-resolved absorption feature at 3.6 THz. The index of refraction showed remarkably little dispersion, changing by only 0.0001 over the range from 0.5 to 4.5 THz.

These results are quite encouraging for the development of FZ-Si single-mode THz fiber and ribbon waveguides[18,19] of up to 100-cm length for which power absorption coefficients of less than 0.025/cm would be obtained for frequencies below 2 THz and for which the intrinsic group-velocity dispersion would be negligible. In addition, these measured properties enable excellent transmissive optics of all types.

ACKNOWLEDGMENTS

This work was partially supported by the National Science Foundation, the Department of Energy EPSCoR Program, and the U.S. Army Research Office. D. Grischkowsky's e-mail address is grischd@ceat.okstate.edu.

REFERENCES

1. C. M. Randall and R. D. Rawcliffe, "Refractive indices of germanium, silicon, and fused quartz in the far-infrared," Appl. Opt. **6**, 1889–1894 (1967).
2. E. V. Loewenstein, D. R. Smith, and R. L. Morgan, "Optical constants of far infrared materials. Crystalline solids," Appl. Opt. **12**, 398–406 (1973).
3. W. R. Passchier, D. D. Honijk, M. Mandel, and M. N. Afsar, "A new method for the determination of complex refractive index spectra of transparent solids in the far-infrared spectral region; results of pure silicon and crystals quartz," J. Phys. D **10**, 509–517 (1977).
4. J. R. Birch, "The absolute determination of complex reflectivity," Infrared Phys. **18**, 613–620 (1978).
5. A. K. Wan Abdullah, K. A. Maslin, and T. J. Parker, "Observation of two-phonon difference bands in the FIR transmission spectrum of Si," Infrared Phys. **24**, 185–188 (1984).
6. M. N. Afsar, "Dielectric measurements of millimeter-wave materials," IEEE Trans. Microwave Theory Tech. **MTT-32**, 1598–1609 (1984).
7. J. M. Dutta, C. R. Jones, and H. Dave, "Complex dielectric constants for selected near-millimeter-wave materials at 245 GHz," IEEE Trans. Microwave Theory Tech. **MTT-34**, 932–936 (1986).
8. T. Ohba and S. Ikawa, "Far-infrared absorption of silicon crystals," J. Appl. Phys. **64**, 4141–4143 (1988).
9. K. Seeger, "Microwave dielectric constants of silicon, gallium arsenide, and quartz," J. Appl. Phys. **63**, 5439–5443 (1988).
10. D. Grischkowsky, S. Keiding, M. van Exter, and Ch. Fattinger, "Far-infrared time-domain spectroscopy with terahertz beams of dielectrics and semiconductors," J. Opt. Soc. Am. B **7**, 2006–2015 (1990).
11. M. van Exter and D. Grischkowsky, "Carrier dynamics of electrons and holes in moderately-doped silicon," Phys. Rev. B **41**, 12140–12149 (1990).
12. M. N. Asfar and H. Chi, "Millimeter wave complex refractive index, complex dielectric permittivity and loss tangent

of extra high purity and compensated silicon," Int. J. Infrared Millim. Waves **15**, 1181–1188 (1994).
13. Tae-In Jeon and D. Grischkowsky, "Nature of conduction in doped silicon," Phys. Rev. Lett. **78**, 1106–1109 (1997).
14. Tae-In Jeon and D. Grischkowsky, "Observation of a Cole–Davidson type complex conductivity in the limit of very low carrier densities in doped silicon," Appl. Phys. Lett. **72**, 2259–2261 (1998).
15. J. Lesurf, *Millimeter-Wave Optics, Devices and Systems* (Hilger, Bristol, UK, 1990).
16. M. T. Reiten, S. A. Harmon, and R. A. Cheville, "Terahertz beam propagation measured through three-dimensional amplitude profile determination," J. Opt. Soc. Am. B **20**, 2215–2225 (2003).
17. L. Duvillaret, F. Garet, and J.-L. Coutaz, "Highly precise determination of optical constants and sample thickness in terahertz time-domain spectroscopy," Appl. Opt. **38**, 409–415 (1999).
18. S. P. Jamison, R. W. McGowan, and D. Grischkowsky, "Single-mode waveguide propagation and reshaping of sub-ps terahertz pulses in sapphire fibers," Appl. Phys. Lett. **76**, 1987–1989 (2000).
19. R. Mendis and D. Grischkowsky, "Plastic ribbon THz waveguides," J. Appl. Phys. **88**, 4449–4451 (2000).